Numerical study on the effect of Lüders plateau on the ductile crack growth resistance of SENT specimens

Shengwen Tu, Xiaobo Ren, Jianying He, Zhiliang Zhang

Abstract

The increasing demand of energy prompts the petroleum industry exploitation activities to the Arctic region where the low temperature is a strong challenge, both for structural design and material selection. For structural materials exhibiting Lüders plateau, it has been reported that lowering temperature will increase the Lüders plateau length. In order to obtain a deep understanding of the Lüders plateau effect on ductile crack growth resistance, we performed numerical analyses with SENT specimens and the Gurson damage model. The Lüders plateau was simplified by keeping the flow stress constant and varying the plateau length. The results show that the existence of Lüders plateau does not influence the initiation toughness, however, will alter the material's fracture resistance significantly. It is found that the Lüders plateau effect is in general controlled by the stress triaxiality level in front of the crack tip. Both the strain hardening and the crack depth effects on resistance curves are alleviated due to the Lüders plateau. For materials with very small initial void volume fraction the Lüders plateau effect is more pronounced. Since the Lüders plateau intensifies the crack driving force and may lower down crack resistance curve, special attention should be paid for the application of materials with Lüders plateau in the Arctic.

Keywords: Lüders plateau; ductile crack growth; resistance curve; constraint; stress triaxiality.

Funding Information

Chinese Scholarship Council; Research Council of Norway, Grant/Award Number: 228513/E30.

S. Tu
Department of Structural Engineering, Norwegian University of Science and Technology (NTNU), Trondheim 7491, Norway

X. Ren
SINTEF Industry, Trondheim 7456, Norway

J. He
Department of Structural Engineering, Norwegian University of Science and Technology (NTNU), Trondheim 7491, Norway

Z. Zhang (Corresponding Author)
Department of Structural Engineering, Norwegian University of Science and Technology (NTNU), Trondheim 7491, Norway.
ORCID: 0000-0002-9557-3455
E-mail: zhiliang.zhang@ntnu.no

1. Introduction

The Arctic has become an interesting region to petroleum industry, considering its abundant undiscovered oil and gas reserves. The assessment conducted by the United States Geological Survey indicates that about 30% of the world's undiscovered gas and 13% of the world's undiscovered oil may be located in that region (Gautier et al., 2009). However, many factors may affect the exploitation activities, including harsh environment, heavy drilling and shipping cost, as well as climate considerations (Ermida, 2014; Harsem et al., 2011). The low temperature appears to be a key challenge for the design and assessment of the infrastructures to be built in the Arctic region. It is well-known that most structural steels show obvious temperature dependent mechanical properties, such as yield stress, ductile-brittle fracture transition behavior. Previous investigations demonstrate that for some steels, the so-called Lüders plateau which is influenced by loading rate, ferrite grain size, yield stress, et al. may occur in uniaxial tension test (Beardsmore et al., 2013; Dahl et al., 2018; Hallai and Kyriakides, 2013; Han et al., 2017; Liu et al., 2015; Mazière et al., 2017; Ren et al., 2015; Tsuchida et al., 2006). It has been reported that lowering testing temperature will increase the Lüders plateau length, see Fig. 1. Ren et al. performed tensile tests of a 420MPa structural steel with temperatures varying from 0 to -90 ℃ and created a relation between temperature and the Lüders plateau length (Ren et al., 2015). Dahl numerically investigated the effect of the yield stress and Lüders plateau length on crack driving force with single edge notched tensile (SENT) specimens and found that the increasing yield stress and Lüders plateau length will intensifies the crack driving force (Dahl et al., 2018). In Dahl's work, a horizontal plateau was used to simplify the Lüders behavior. The purpose in the present study is to investigate the effect of Lüders plateau length on the ductile crack growth resistance. The simplification of the Lüders behavior in Dahl's work is followed in this study.

For elastoplastic fracture, which is the focus in this paper, *J*-integral and crack tip opening displacement (CTOD) are widely used to characterize material's fracture toughness (Eikrem et al., 2008; Han et al., 2014; Henry and Luxmoore, 1997; Østby et al., 2007a, b). The specimen size (Xu et al., 2009; Zhao et al., 2014), geometry, loading type (Cravero and Ruggieri, 2005) et al. influence the crack tip stress field. The deviation of crack tip stress field from the reference one is now generally understood as the crack tip constraint. By introducing a second parameter to characterize the constrain level, the value of fracture toughness can be transferred from one specimen geometry to another. O'Dowd and Shih (O'Dowd and Shih, 1991, 1992) proposed a *J-Q* formulation to characterize the crack tip stress and strain fields. In their formulation, *J-integral* sets the size scale over which large stresses and strains develop, while *Q* is the constraint parameter to scale the near-tip stress distribution and the stress triaxiality ahead of the

crack. The formulation was further extended by Zhang et al. by introducing a parameter M to characterize material mismatch (Zhang et al., 1997; Zhang et al., 1996).

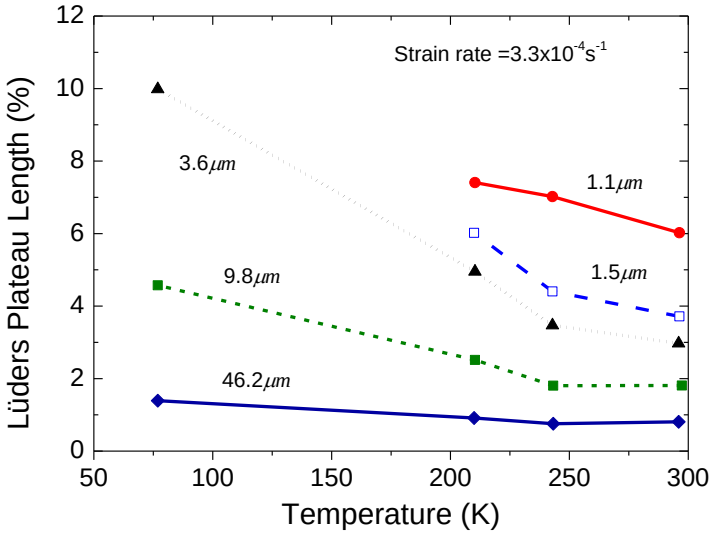

Fig. 1 Temperature dependence on Lüders plateau for materials with various ferrite grain sizes (*Tsuchida et al., 2006*).

For ductile fracture, the crack resistance curve is used to characterize the material's ability to resist crack extension. The resistance can be characterized by the *J*-integral or CTOD. The resistance curve is usually measured with compact tension specimen, single edge bending specimen or SENT specimen. The behavior of resistance curve is also affected by the crack tip constraint level (Xu et al., 2010), as well as the material's mechanical (hardening) and damage parameters (initial void volume fraction). The effects of specimen geometry, specimen size, loading type, pre-strain (Eikrem et al., 2008) et al. on crack resistance curve have been widely investigated. However, studies on the effect of low temperature induced Lüders plateau on ductile crack growth are very limited, if available.

It should be noted that a pipeline usually have two failure modes, namely the tension failure with possibly a defect (crack), and compression failure by wrinkling or buckling. Lüders plateau may have strong influence on both failure modes (Hallai and Kyriakides, 2011a, b). In order to limit the scope, tension failure with crack is the focus of this study. To obtain a deep understanding of the effect of Lüders plateau length on ductile crack growth resistance, we performed a series of numerical analyses with SENT specimen. The Gurson damage model introduced in section 2 was used to simulate the crack growth. A family of Lüders plateau length ranging from 0 to infinite，representing two limit material models (material without Lüders plateau and the perfectly plastic material), was investigated. More

information about the numerical procedure and material properties are presented in section 3. Discussions on effects of the crack depth, Lüders plateau length, strain hardening, as well as the initial void volume fraction on the resistance curve are discussed in section 4. Concluding remarks are presented in section 5.

2. The Gurson damage model

The mechanism of ductile fracture failure in metallic materials is widely acknowledged as the micro voids nucleation, growth and coalescence. Gurson (Gurson, 1977) proposed a constitutive model for ductile materials incorporating voids, considering the hydrostatic stress effect on plastic yielding and void growth. The original Gurson damage model was further modified by Tvergaard and Needleman (Tvergaard, 1981, 1982; Tvergaard and Needleman, 1984). Finally the yield surface has the following form and known as Gurson-Tvergaard-Needleman model:

$$\phi\left(q,\sigma_f,f,\sigma_m\right)=\frac{q^2}{\sigma_f^2}+2q_1 f\cosh\left(\frac{3q_2\sigma_m}{2\sigma_f}\right)-1-(q_1 f)^2=0 \tag{1}$$

where q is von Mises stress, σ_f is the flow stress of the matrix material and is a function of equivalent plastic strain. σ_m is the mean stress; q_1 and q_2 are the parameters introduced by Tvergaard; f is the void volume fraction. In this study, $q_1=1.5$ and $q_2=1$ are used for all the numerical analyses.

The Gurson damage model has gained wide attentions and some new extended versions have been developed. By introducing the competition of homogeneous void growth model and the Thomason's plastic limit load model, a so-called complete Gurson model which can not only simulate the void nucleation, growth and, but also the coalescence process without a pre-selected critical void volume fraction was developed by Zhang (Zhang et al., 2000; Zhang, 1996). Based on the Gurson-Tvergaard-Needleman model, Grange and Besson proposed a model taking into account plastic anisotropy and visco-plasticity to model the ductile fracture of Zircaloy-4 sheets (Grange et al., 2000). Nahshon and Hutchinson developed an extended model by incorporates damage growth under low triaxiality straining for shear-dominated states (Nahshon and Hutchinson, 2008).

In this study, the increase of the void volume fraction is solely contributed by the void growth and no void nucleation is considered during loading. Due to the incompressible nature of the matrix material, the void volume increment can be expressed as:

$$df_{growth}=(1-f)d\varepsilon^p:\mathbf{I} \tag{2}$$

where ε^p is the plastic strain tensor and **I** is the second-order unit tensor. When the void volume fraction reaches to the critical value f_c, void coalescence occurs. In this study, an arbitrary value, $f_c = 0.02$, is used for all the analyses. Tvergaard and Needleman introduced a function to simulate void coalescence:

$$f^* = \begin{cases} f & for \quad f \le f_c \\ f_c + \dfrac{f_u^* - f_c}{f_F - f_c}(f - f_c) & for \quad f > f_c \end{cases} \tag{3}$$

where $f_u^* = 1/q_1$. When the condition $f > f_c$ is satisfied, f^* replaces f in Eq. (1). As the void volume fraction increases to f_F, the element is assumed to lose load carrying capacity and cracks are expected to propagate. An empirical equation, $f_F = 0.2 + 2f_0$, is considered in this study.

3. Numerical Procedure

3.1 Materials properties

In this study, flow stress-strain curve of the matrix material is described by the following rule:

$$\sigma_f = \begin{cases} \sigma_0 & for \quad \overline{\varepsilon^p} \le \varepsilon_L \\ \sigma_0 (1 + \dfrac{\overline{\varepsilon^p} - \varepsilon_L}{\varepsilon_0})^n & for \quad \overline{\varepsilon^p} > \varepsilon_L \end{cases} \tag{4}$$

where σ_0, ε_0 and n are the yield stress, yield strain and strain hardening exponent, respectively. For all the numerical analyses, $\sigma_0 = 400\ MPa$, Young's modulus $E = 200\ GPa$ and the Poisson ratio $v = 0.3$ were used. $\overline{\varepsilon^p}$ and ε_L are the equivalent plastic strain and the Lüders strain. A horizontal plateau is used to model the Lüders behavior and the stress is assumed to equal to the yield stress. When $\varepsilon_L = 0$, the matrix material returns to follow the power-law hardening rule. Flow stress-strain curve for material with $n = 0.1$ and $\varepsilon_L = 0.05$ is displayed in Fig. 2, as described by Eq. (4).

3.2 Numerical procedure

In the present study, SENT specimens are chosen to study the effect of Lüders plateau on ductile crack growth with ABAQUS 6.12. The geometry of the SENT specimen is schematically shown in Fig. 3. A fixed specimen width, $W = 50\ mm$, is used for all the analyses. Xu and Østby found that the crack resistance curve depends significantly on the specimen width (Østby et al., 2007a, b; Xu et al., 2009). However, the specimen size effect is out of the scope of this study and will not be focused. The specimen length L is 10 times of the specimen width. a is the initial crack length. The crack depth effect is investigated by varying the ratio of the initial crack length to the specimen width, a/W.

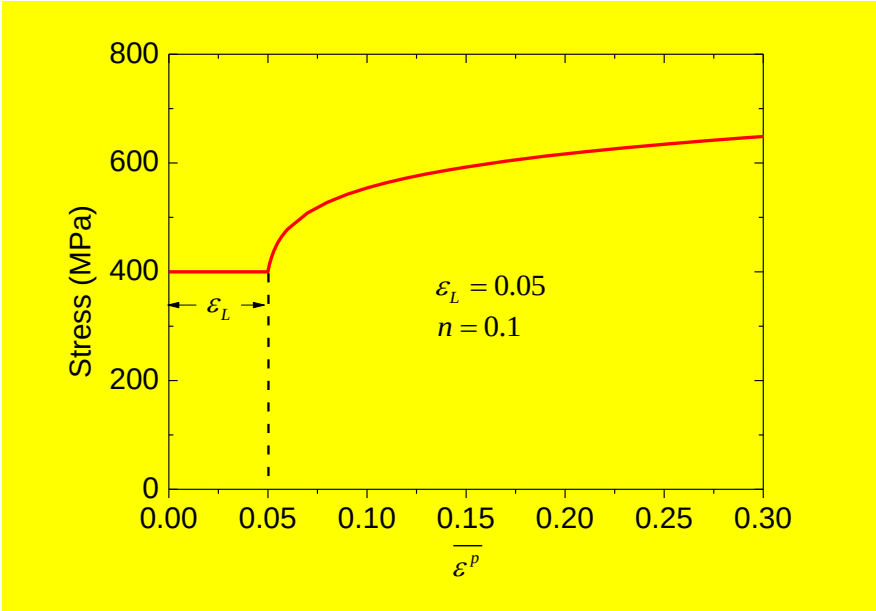

Fig. 2 Illustration of simplified Lüders plateau on flow stress-strain curve according to Eq. (4).

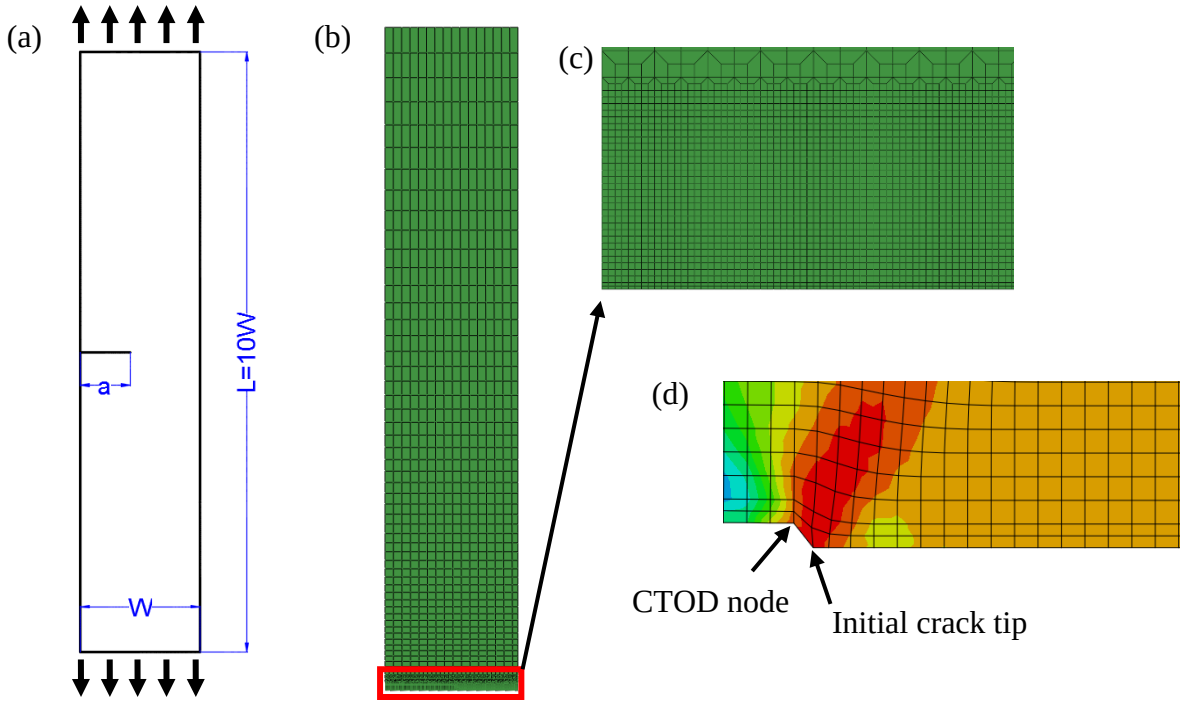

Fig. 3 (a) SENT specimen; (b) Global mesh; (c) Local mesh; (d) Definition of CTOD node.

Considering the symmetry of the problem, only one half of the specimen is modeled. 4-node reduced integration plane strain elements (CPE4R) are applied. Large deformation is accounted for all the analyses. A remote homogeneous displacement boundary condition is applied to induce crack propagation. The region with uniform mesh size, see Fig. 3 (b) and (c), is extended to 3.0 *mm* above the symmetric plane with mesh size of $0.1 \times 0.1\ mm$, except two rows of elements with mesh size of

$0.1 \times 0.05\ mm$ at the symmetric plane where the crack is supposed to propagate. Indeed, mesh size will affect the predicted resistance curve. For real materials, the mesh size should be determined by comparing the resistance curves from experiments and numerical predictions. In this study, we qualitatively investigate the Lüders length effect on ductile crack growth and the mesh size effect is not considered. The remaining part of the specimen is meshed with relative coarse elements, see Fig. 3 (b). When the void volume fraction reached f_F, the element failed and the crack extension is measured by multiplying the original element length ($0.1\ mm$) with the failed element numbers. Corresponding CTOD is measured as 2 times of the displacement of the node neighbor to the initial crack tip, see Fig. 3 (d).

4. Results and discussion

4.1 Lüders plateau effect on crack resistance curves

The crack resistance curves from numerical analyses with the Gurson damage model are presented in Fig. 4. The strain hardening exponent and the initial void volume fraction used in this section are $n = 0.05$ (corresponding to yield tensile ratio *Y/T*=0.85) and $f_0 = 0.005$. The length of Lüders plateau studied varies from 0 to infinite, considering the two limit cases: strain hardening without Lüders plateau and the perfectly plastic material. Lüders plateau length effect can be clearly observed in Fig. 4. For the SENT specimen with $a/W = 0.1$, as can be seen in Fig. 4 (a), with the increase of Lüders plateau length, the resistance curve lowers down firstly; up to the case with $\varepsilon_L = 0.05$, the resistance curve starts to shift up with the increase of ε_L. For $\varepsilon_L = 0.03$ and $\varepsilon_L = 0.05$, the corresponding resistance curves almost overlap to each other in the range of crack growth up to 3 mm. It can also be observed that only for $\varepsilon_L = 0.2$ and $\varepsilon_L = \text{infi}$, the resistance curves are higher than the reference case with $\varepsilon_L = 0$ in Fig. 4 (a). Similar observation can be found in Fig. 4 (b) and Fig. 4 (c) for SENT specimens with $a/W = 0.3$ and $a/W = 0.5$. Compared with the resistance curves in Fig. 4 (a), it can be found that the value of ε_L corresponding to the lowest resistance curve decreases with the increase of crack depth in Fig. 4 (b) and Fig. 4 (c). In Fig. 4 (b), when $\varepsilon_L \geq 0.1$ the resistance curves appear to be higher than the reference material without Lüders plateau; while in Fig. 4 (c), same phenomenon can be seen when $\varepsilon_L \geq 0.07$. It can also be found that in Fig. 4 (b) and (c), with the increase of crack growth, the resistance curves for $\varepsilon_L = 0.2$ are even slightly higher than those from the perfectly plastic material at $\Delta a \leq 3\ mm$. Fig. 4 indicates that the crack depth plays a significant role on the effect of Lüders plateau length on the crack resistance curve. Usually, the crack resistance curve is dominated by the constraint level ahead of the

crack tip. The resistance curve for cracks under higher constraint level is relatively lower than that under lower constraint level, and vice versa (Nourpanah and Taheri, 2011; Xu et al., 2010). Fig. 4 suggests that the existence of the Lüders plateau influences the constraint level, and the effect of Lüders plateau length is also dependent of the specimen geometry constraint level (crack depth here).

The resistance curves in Fig. 4 are then regrouped by the Lüders plateau length and are presented in Fig. 5. As can be seen in Fig. 5 (a) that for the reference material case with $\varepsilon_L = 0$, the resistance curves show obvious crack depth dependence: resistance curve lowers down with the increase of crack depth (Xia et al., 1995; Xu et al., 2009). It has been known that for deeper cracked specimen the constraint ahead of the crack tip is relatively higher. For the materials with same Lüders plateau in Fig. 5 (b)-(g), it can be seen that the gap between the resistance curves decreases with the increase of the plateau length. Especially, the resistance curves in Fig. 5 (c)-(g) are very close to each other, displaying minor crack depth dependence. It is shown that the existence of the Lüders plateau alleviates the crack depth effect. For $\varepsilon_L = \text{infi}$ in Fig. 5 (h), the crack depth effect plays a dominate role on the resistance curves and obvious difference between the crack resistance curves can be noticed.

To understand the Lüders plateau effect on the ductile crack growth resistance, we further investigate the void volume evolution at given crack growth. In Fig. 6 (a), values of CTOD at crack growth $\Delta a = 0.1,\ 0.5$ and 1 *mm* are plotted against the Lüders plateau length with $a/W = 0.1$. In Fig. 6 (b)-(d), the evolution of void volume fraction at the crack tip element corresponding to $\Delta a = 0.1,\ 0.5$ and 1 *mm* is presented with respect to the equivalent plastic strain. It can be seen that at crack initiation ($\Delta a = 0.1$ *mm*), the value of CTOD increases slightly with the increase of Lüders plateau length. Correspondingly, the evolution of void volume fraction shows relative small dependence on Lüders plateau length, as seen in Fig. 6 (b). The equivalent plastic strain at the maximum volume fraction increases slightly with the increase of the Lüders plateau length. It should be noted that, when the crack tip element fails (reaching the void volume fraction at separation) at smaller equivalent plastic strain, the corresponding CTOD will be smaller. The void volume fraction evolution in Fig. 6 (b) well explains the slight increase of CTOD with the increase of Lüders plateau length in Fig. 6 (a) at crack initiation.

At crack growth $\Delta a = 0.5\,mm$, it can be noticed that the values of CTOD in Fig. 6 (a) firstly decrease with the increase of Lüders plateau length and then increase. The void volume fraction evolution of the element corresponding to $\Delta a = 0.5$ *mm* for all the cases is plotted against equivalent plastic strain in Fig. 6 (c). It is straightforward that void volume fraction evolution and the equivalent plastic strain at failure are different to each other. For $\varepsilon_L = 0.03$, the void volume fraction grows faster than other cases

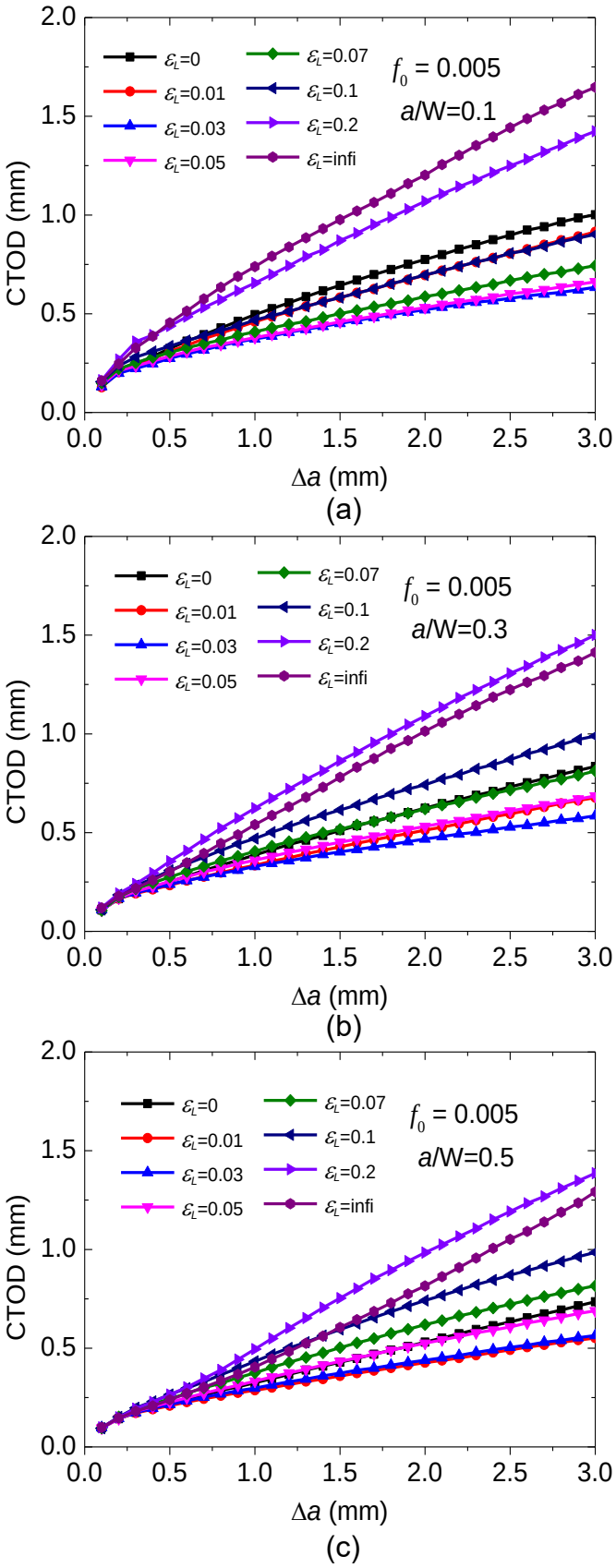

Fig. 4 The Lüders plateau length effect on the resistance curves of SENT specimen with n=0.05; (a) a/W=0.1; (b) a/W=0.3; (c) a/W=0.5.

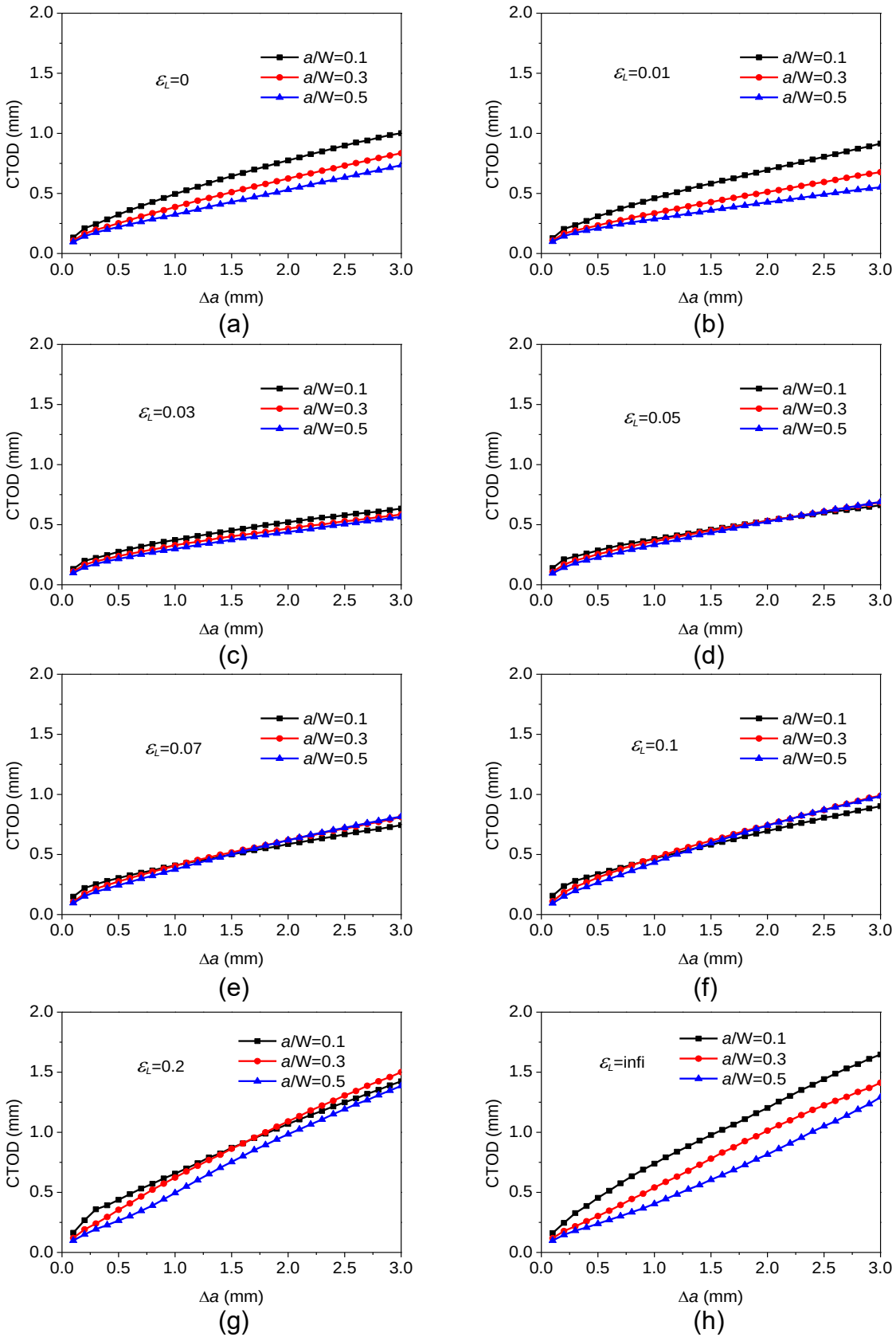

Fig. 5 Crack depth effect on the resistance curves of SENT specimen for materials with $n = 0.05$ *and different Lüders plateau length; (a)* $\varepsilon_L = 0$ *; (b)* $\varepsilon_L = 0.01$*; (c)* $\varepsilon_L = 0.03$*; (d)* $\varepsilon_L = 0.05$*; (e)* $\varepsilon_L = 0.07$ *; (f)* $\varepsilon_L = 0.1$*; (g)* $\varepsilon_L = 0.2$ *; (h)* $\varepsilon_L = \text{infi}$.

and fails at smaller equivalent plastic strain. As a result of this, the corresponding CTOD is smaller. For all the cases in Fig. 6 (c), only for $\varepsilon_L \geq 0.1$, the equivalent plastic strains at failure are larger than $\varepsilon_L = 0$. It can be seen in Fig. 6 (a) that when $\varepsilon_L \geq 0.1$, the values of CTOD are larger than $\varepsilon_L = 0$. Otherwise, the corresponding values of CTOD are smaller than the reference case with $\varepsilon_L = 0$. The sequence of equivalent plastic strains at failure in Fig. 6 (c) agrees well with the distribution of CTOD in Fig. 6 (a) for $\Delta a = 0.5\,mm$. Similar results can be found at $\Delta a = 1\,mm$ in Fig. 6 (d).

For $a/W = 0.3$ and $a/W = 0.5$, CTODs at crack growth $\Delta a = 0.1,\ 0.5$ and 1 *mm* are plotted against the Lüders plateau length and are presented in Fig. 7 and Fig. 8, together with void volume fraction evolution of the corresponding current crack tip elements. Similar observations can be found in Fig. 7-8 as those found in Fig. 6. It is noticed that for $a/W = 0.3$, the evolution of void volume fraction almost collapse into one for all the cases analyzed in Fig. 7 (b), indicating that the Lüders plateau length has no effect on crack initiation toughness. The same results can be seen in Fig. 8 for $a/W = 0.5$. Results in Fig. 6-8 demonstrate that the value of CTOD at crack initiation is not influenced by Lüders plateau length for the cases analyzed. It can also be noticed that for $\varepsilon_L = 0.2$ with $a/W = 0.3$ and $a/W = 0.5$, the values of CTOD at $\Delta a = 0.5$ and 1 *mm* are even higher than those of the perfectly plastic material, because of the delayed void volume fraction evolution for $\varepsilon_L = 0.2$, as seen in Fig. 7 (c)-(d) and Fig. 8 (c)-(d).

To further study the effect of Lüders plateau length on ductile crack growth, the stress triaxiality evolution of the crack tip elements corresponding to $\Delta a = 0.5\,\text{mm}$ with $a/W = 0.1$ is plotted against the equivalent plastic strain in Fig.8. It can be seen for all the cases analyzed, the stress triaxiality increases slightly and then decrease with the increase of equivalent plastic strain. It has been shown that the equivalent plastic strain at failure, ε^f, depends significantly on the stress state (Bai et al., 2009; Bao and Wierzbicki, 2004; Tu et al., 2018). In some studies (Bao and Wierzbicki, 2004; Tu et al., 2018), an average stress triaxiality, T^*, which considering the loading history, has been used to characterize the constraint, Eq. (5):

$$T^* = \int_0^{\varepsilon_f} T(\varepsilon) \cdot d\varepsilon \Big/ \varepsilon^f \tag{5}$$

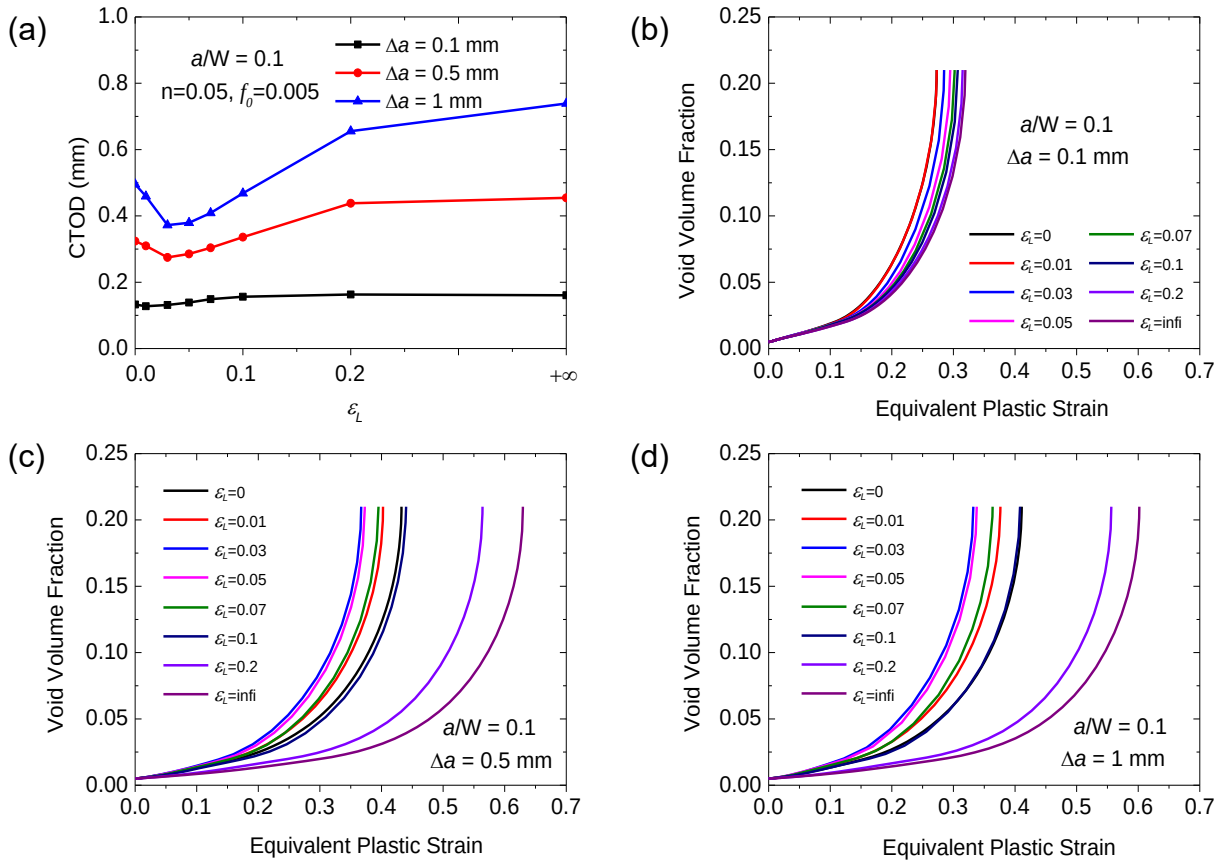

Fig. 6 (a) CTOD vs. Lüders plateau length at $\Delta a = 0.1$, 0.5 and 1 mm with $a/W = 0.1$*; (b) Evolution of void volume fraction of current crack tip element corresponding to* $\Delta a = 0.1\,\text{mm}$; *(c) Evolution of void volume fraction of current crack tip element corresponding to* $\Delta a = 0.5\,\text{mm}$; *(d) Evolution of void volume fraction of current crack tip element corresponding to* $\Delta a = 1\,\text{mm}$.

In the following, the value of the average stress triaxiality in Fig. 9 for each case is calculated by Eq. (5) and shown in Fig. 10 as a function of Lüders plateau length. Values of the average stress triaxiality of the elements at $\Delta a = 1$ *mm* for SENT specimen with $a/W = 0.5$ are also presented. It can be seen in Fig. 10 that for SENT specimens with $a/W = 0.1$ at $\Delta a = 0.5$ *mm*, the average stress triaxiality shows opposite trend in Fig. 6 (a), indicating that fracture toughness under higher constraint tends to be lower. This also applies for SENT specimens with $a/W = 0.5$ at $\Delta a = 1$ *mm*, as shown by the red curve in Fig. 10 and blue curve in Fig. 8 (a). It can be inferred that Lüders plateau alters the crack tip constraint.

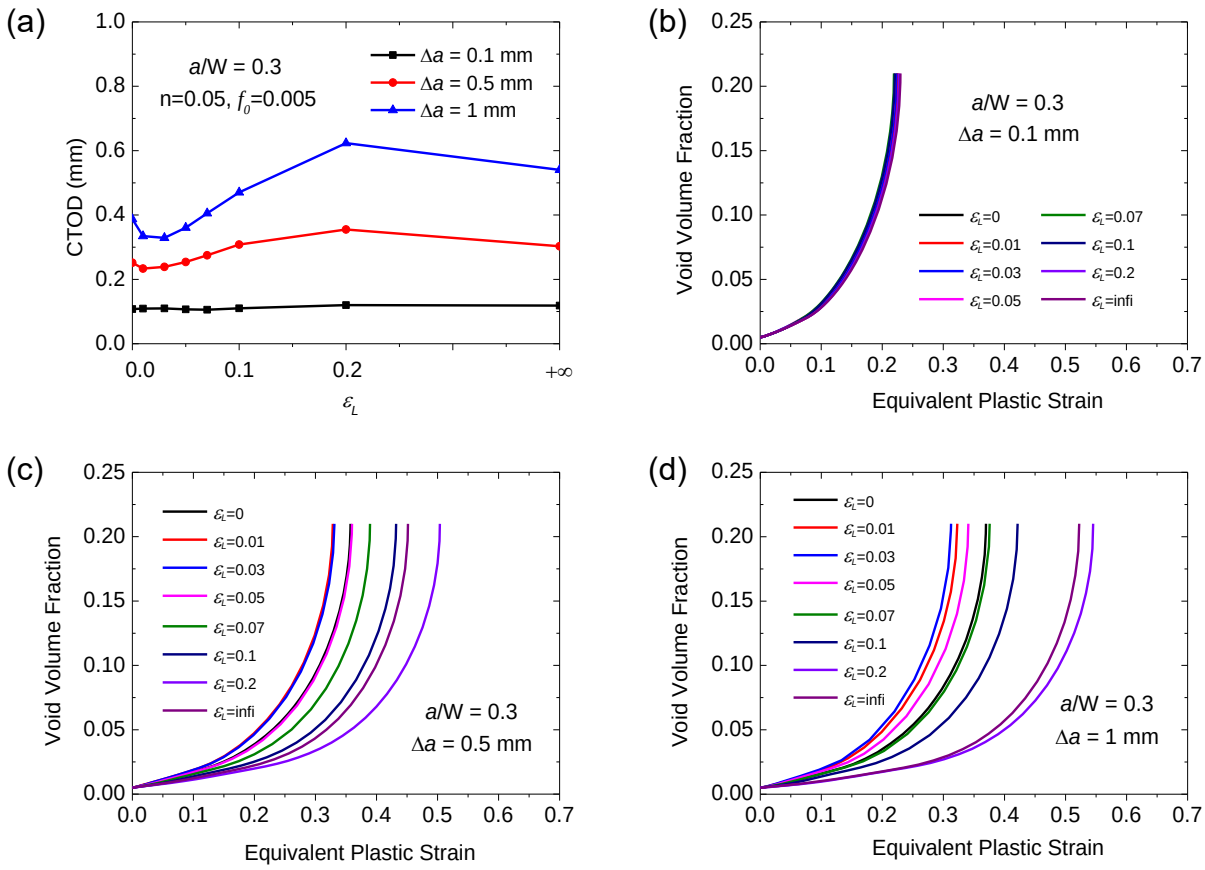

Fig. 7 (a) CTOD vs. Lüders plateau length at $\Delta a = 0.1$, 0.5 and 1 mm with $a/W = 0.3$*; (b) Evolution of void volume fraction of the current crack tip element corresponding to* $\Delta a = 0.1$ mm; *(c) Evolution of void volume fraction of the current crack tip element corresponding to* $\Delta a = 0.5$ mm; *(d) Evolution of void volume fraction of the current crack tip element corresponding to* $\Delta a = 1$ mm.

4.2 materials with different strain hardening exponents

It is well acknowledged that the resistance curve is influenced by material's strain hardening. Xia and Shih (Xia and Shih, 1995) have conducted numerical analyses with modified boundary layer model under small scale yielding conditions. They found that the resistance curves for materials with higher strain hardening are considerably higher. Eikrem and Zhang (Eikrem et al., 2008) preformed numerical analyses with the complete Gurson model and SENT specimen. Their results showed that materials with higher strain hardening yielded lower resistance curve. The dependence of crack resistance curve on the strain hardening is contradictory in (Xia and Shih, 1995) and (Eikrem et al., 2008) and the reason behind is still not clear. In this section, we fix all the parameters the same as in section 4.1 and only vary with the strain hardening exponents. The Lüders plateau length varying from 0 to 0.2 is considered. Resistance

curves for SENT specimens with hardening exponents $n = 0.1,\ 0.15$ (corresponding to Y/T=0.67 and 0.52) are presented in Fig. 11 and Fig. 12, respectively. Resistance curves for the perfectly plastic material have also been compared. The effect of Lüders plateau length on the resistance curves in Fig. 4 can also be found in Fig. 11 and Fig. 12. It can also be observed that the values of CTOD at crack initiation are approximately identical for SENT specimens with same geometry and hardening exponent, showing weak dependence on Lüders plateau. Resistance curves for the perfectly plastic material are much higher than those of strain hardening materials, for specimens with the same geometry.

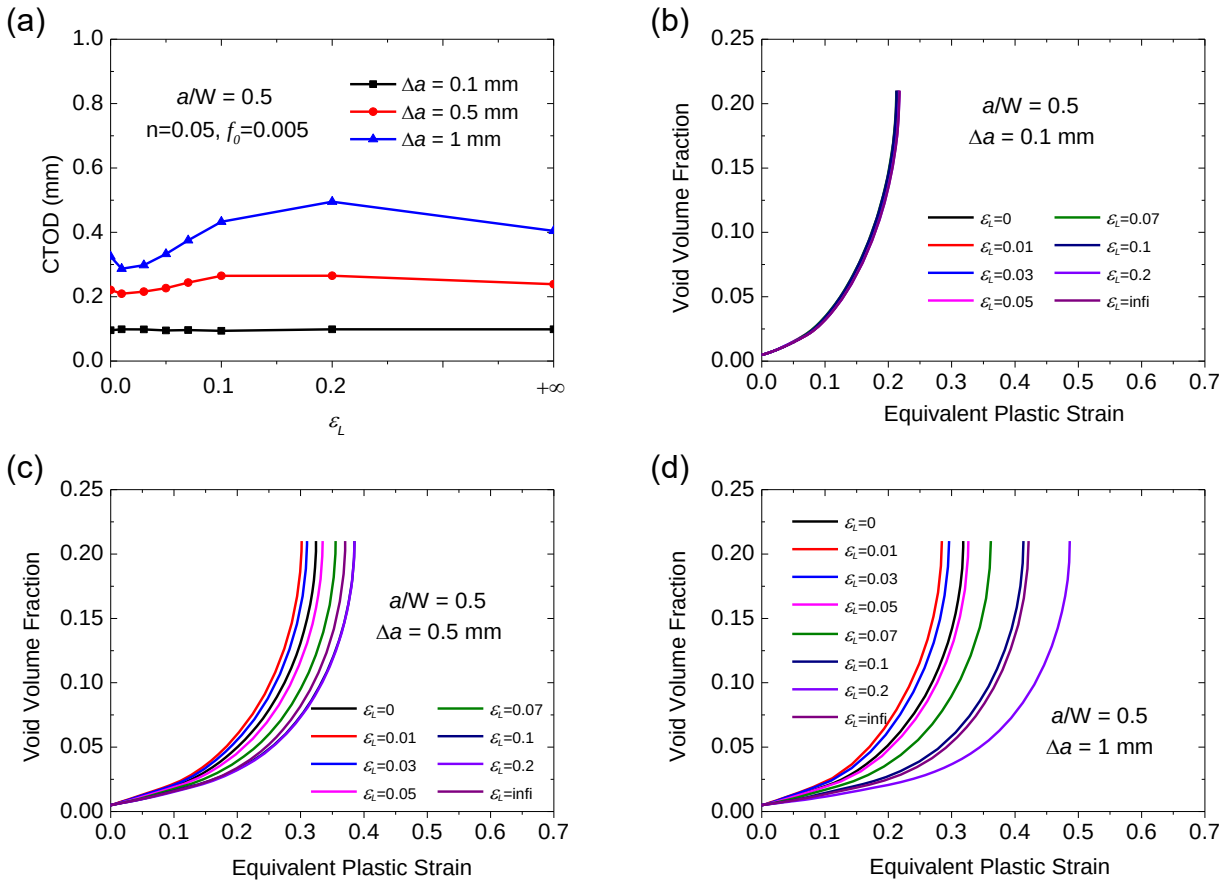

Fig. 8 (a) CTOD vs. Lüders plateau length at $\Delta a = 0.1$, 0.5 and 1 mm with $a/W = 0.5$*; (b) Evolution of void volume fraction of the current crack tip element corresponding to* $\Delta a = 0.1$ mm; *(c) Evolution of void volume fraction of the current crack tip element corresponding to* $\Delta a = 0.5$ mm; *(d) Evolution of void volume fraction of the current crack tip element corresponding to* $\Delta a = 1$ mm.

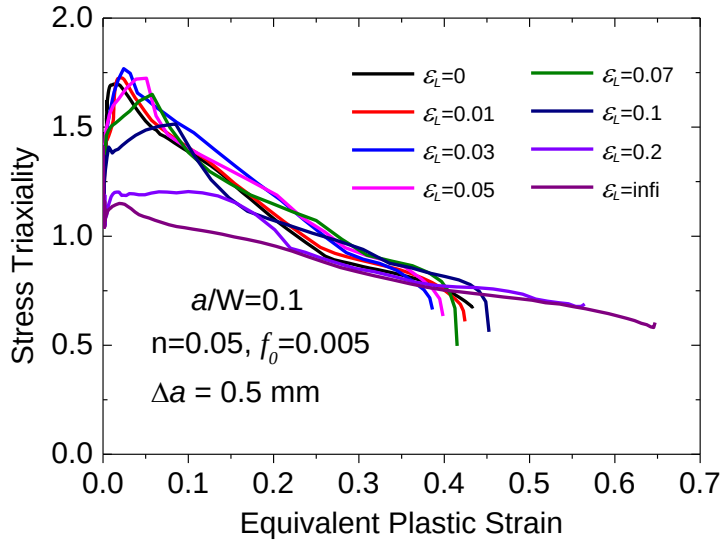

Fig. 9 Stress triaxiality vs. equivalent plastic strain of SENT specimen with a/W=0.1.

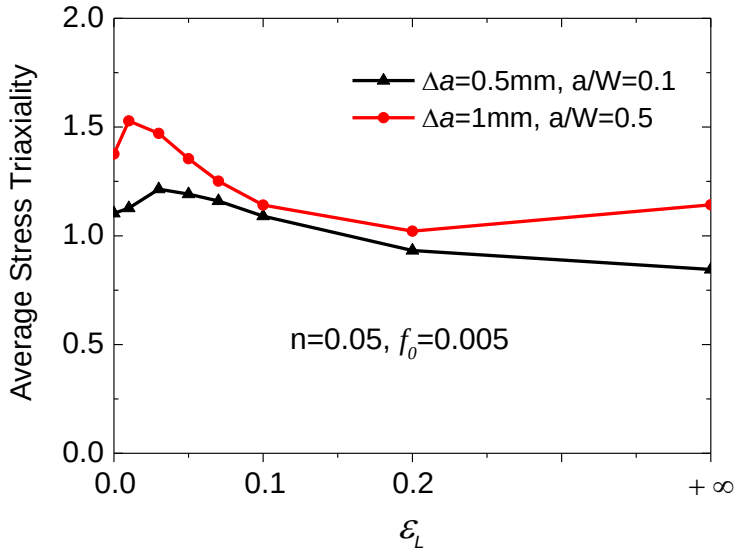

Fig. 10 Average stress triaxiality vs. Lüders plateau length.

Compared with the results in Fig.3, Fig. 11 and Fig. 12, it can be found that for SENT specimens with same geometry, ε_L corresponding to the lowest resistance curve shows slight strain hardening dependence and decreases with higher hardening exponent. It can also be observed that the effect of Lüders plateau length on the resistance curves depends on strain hardening. For specimens with $a/W = 0.1$ and materials with $n = 0.05$, the resistance curves tend to be higher than the reference case ($\varepsilon_L = 0$) when $\varepsilon_L \geq 0.2$; while for materials with $n = 0.1$ and $n = 0.15$, it occurs when $\varepsilon_L \geq 0.1$ and $\varepsilon_L \geq 0.07$, respectively. For specimens with $a/W = 0.3$ and $a/W = 0.5$, same observations can be

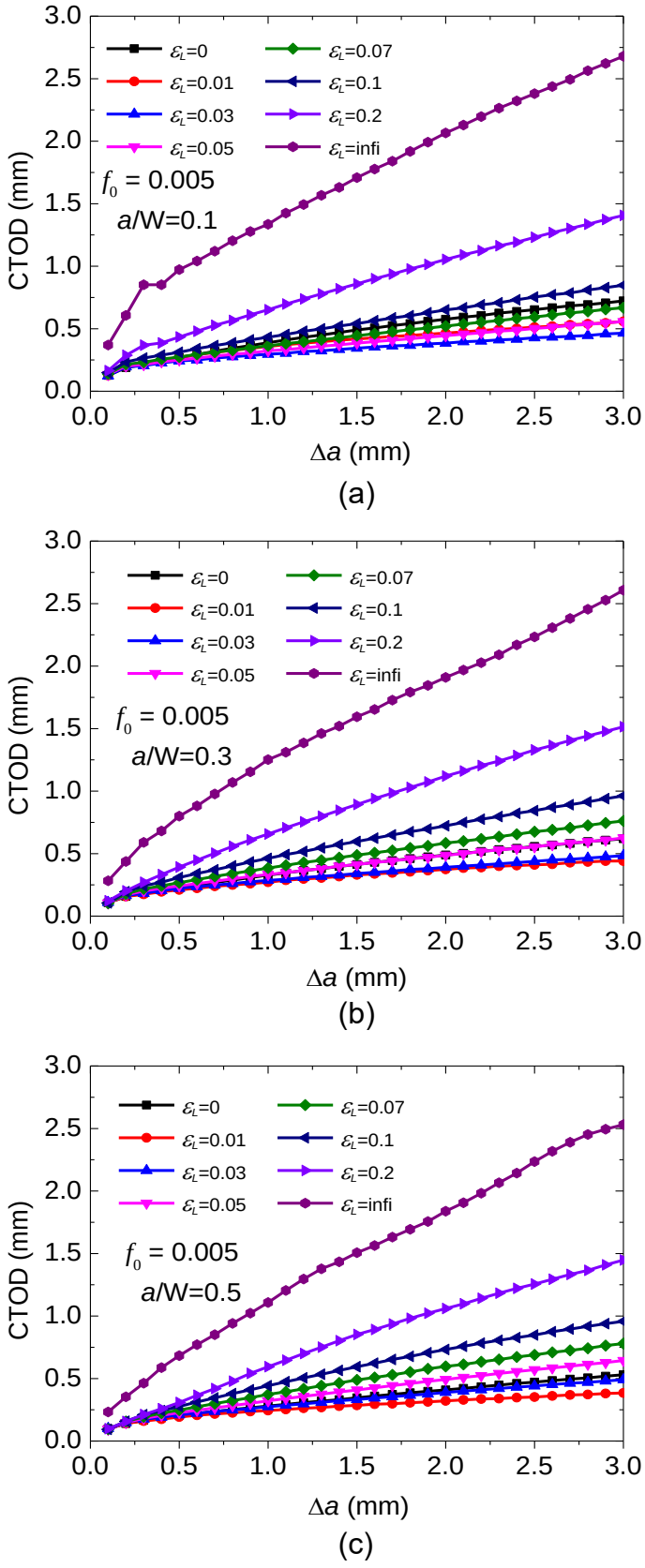

Fig. 11 The Lüders plateau length effect on the resistance curves of SENT specimens with n=0.1; (a) a/W=0.1; (b) a/W=0.3; (c) a/W=0.5.

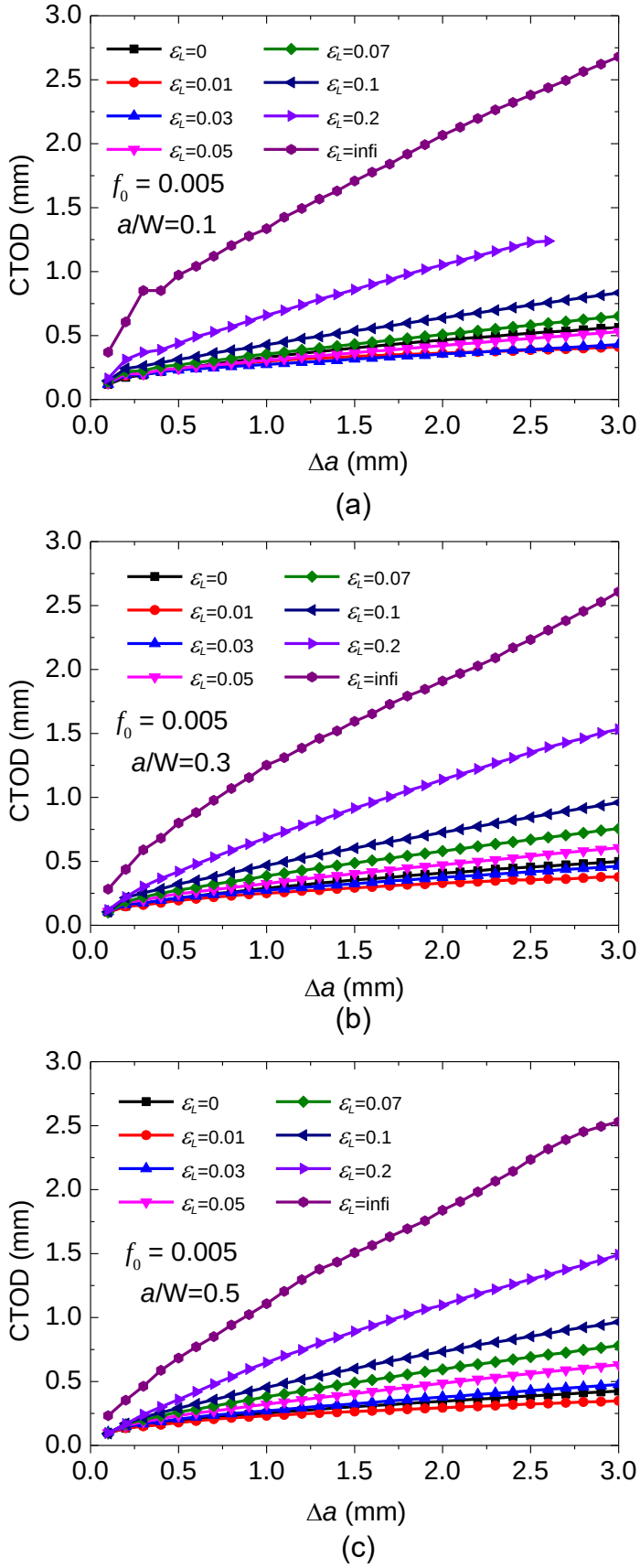

Fig. 12 The Lüders plateau length effect on the resistance curves of SENT specimens with n=0.15; (a) a/W=0.1; (b) a/W=0.3; (c) a/W=0.5.

found. Especially for specimens with $a/W = 0.5$ and materials with $n = 0.15$ in Fig. 12 (c), only for $\varepsilon_L = 0.01$ the resistance is lower than the case with $\varepsilon_L = 0$, otherwise the resistance curve is higher. It can be concluded that Lüders plateau may modify the ductile crack growth, however, the degree of modification depends strongly on the plateau length, crack depth, as well as material's strain hardening.

The resistance curves in Fig. 4, Fig. 11 and Fig. 12 are then regrouped by Lüders plateau length, crack depth in Fig. 13-15. It can be seen that for materials with or without Lüders plateau, the initiation toughness is nearly identical for specimens with the same geometry and Lüders plateau length, showing weak dependence on strain hardening. For $\varepsilon_L = 0$ in Fig. 13-15, a higher resistance curve can be found for material with lower strain hardening exponent, in consistence with previous study (Eikrem et al., 2008). Difference between the resistance curves reduces with increasing crack depth, for $\varepsilon_L = 0$ in Fig. 13-15. For materials with Lüders plateau, strain hardening effect on the crack resistance curves is also observed. In Fig. 13-15, it is shown that with the increase of Lüders plateau length, resistance curves for SENT specimens with different hardening exponents tend to present slight difference, showing weakly strain hardening dependence. Especially, for $\varepsilon_L = 0.2$ in Fig. 13 (g), the resistance curves almost overlap each other when $\Delta a \leq 3$ *mm* for SENT specimens with $a/W = 0.1$. Same results can be found in Fig. 14 (d)-(g) and Fig. 15 (d)-(f). For SENT specimens with given crack depth, the strain hardening effect is reduced due to the Lüders plateau, and larger Lüders plateau corresponds to larger reduction.

4.3 materials with different initial void volume fractions

The effect of the Lüders plateau length on ductile crack growth may also depends on the material toughness level. For this consideration, we have performed numerical analyses, by keeping all the parameters the same in section 4.1 and changing the initial void volume fraction. From the viewpoint of damage mechanics, materials with smaller void volume fraction show higher toughness. In this section, $f_0 = 0.0005$ is used, which is only 10% of the previous value. The materials used in this section are supposed to have higher toughness than the materials used previously in section 4.1. The resistance curves for SENT specimens with $a/W = 0.1$, 0.3 and 0.5 are presented in Fig. 16, with ε_L varying from 0 to infinite.

Compared with the resistance curve for the same specimen geometry and ε_L in Fig. 4, the resistance curve in Fig. 16 is remarkably higher, as expected. Similar to Fig. 4, values of CTOD at crack initiation ($\Delta a = 0.1$ *mm*) in Fig. 16 are approximately insensitive to the Lüders plateau length. In Fig. 16 (a), the resistance curves for the materials with Lüders plateau are lower than the one without Lüders plateau,

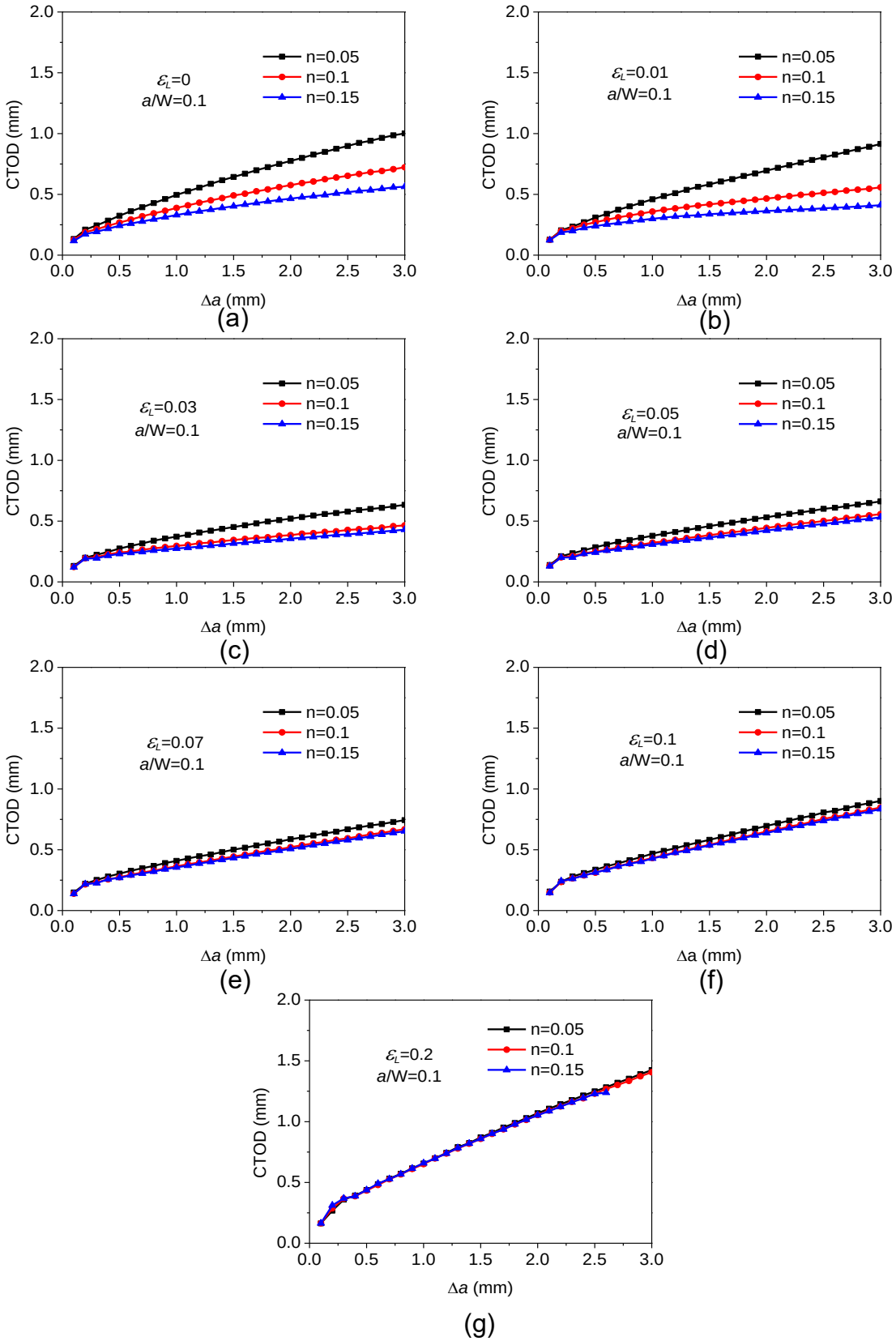

Fig. 13 Resistance curves for SENT specimens with $a/W = 0.1$ *and hardening exponent* $n = 0.05,\ 0.1,\ 0.15$. *(a)* $\varepsilon_L = 0$; *(b)* $\varepsilon_L = 0.01$; *(c)* $\varepsilon_L = 0.03$; *(d)* $\varepsilon_L = 0.05$; *(e)* $\varepsilon_L = 0.07$; *(f)* $\varepsilon_L = 0.1$; *(g)* $\varepsilon_L = 0.2$.

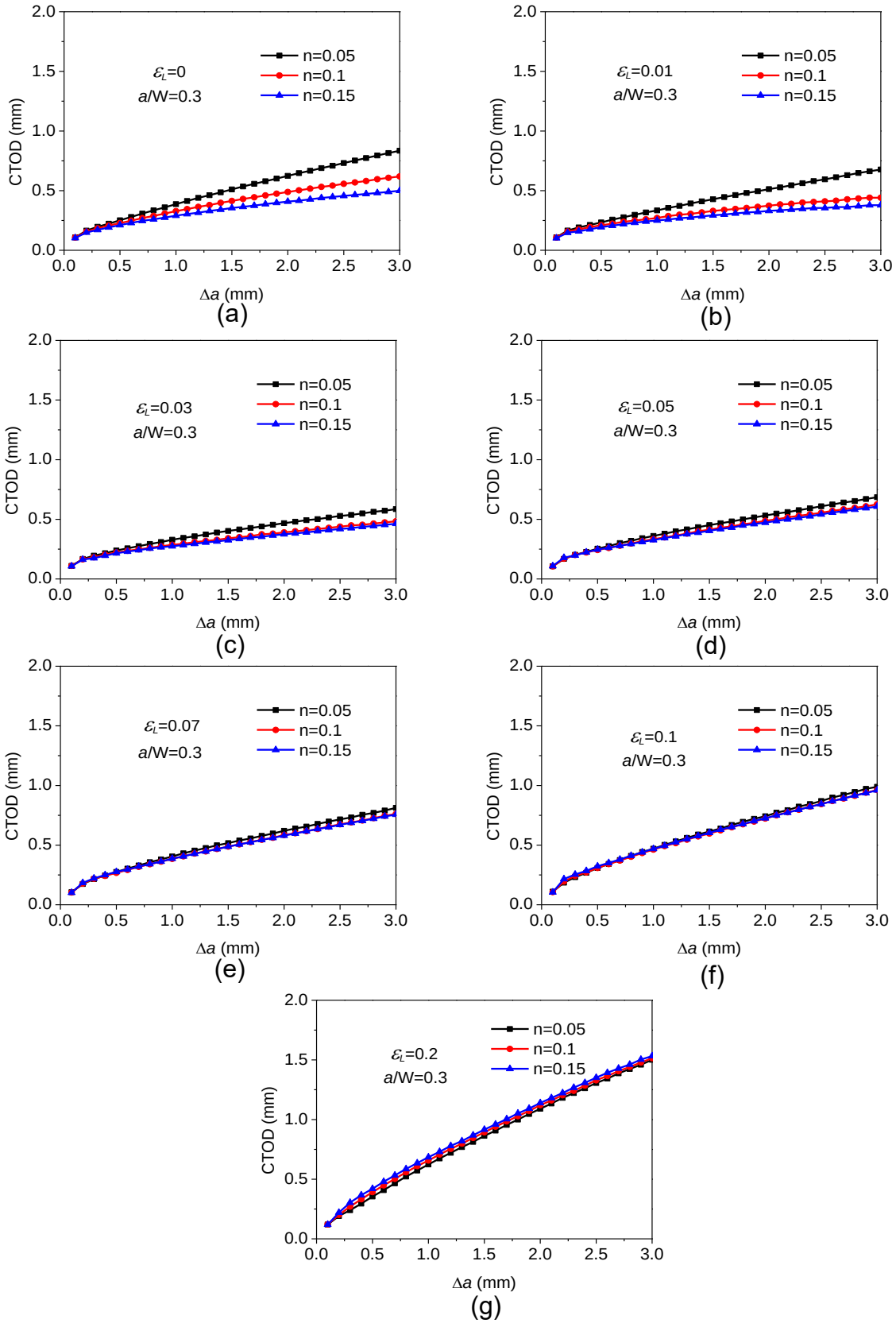

Fig. 14 Resistance curves for SENT specimens with $a/W = 0.3$ *and hardening exponent* $n = 0.05,\ 0.1,\ 0.15$. *(a)* $\varepsilon_L = 0$; *(b)* $\varepsilon_L = 0.01$; *(c)* $\varepsilon_L = 0.03$; *(d)* $\varepsilon_L = 0.05$; *(e)* $\varepsilon_L = 0.07$; *(f)* $\varepsilon_L = 0.1$; *(g)* $\varepsilon_L = 0.2$.

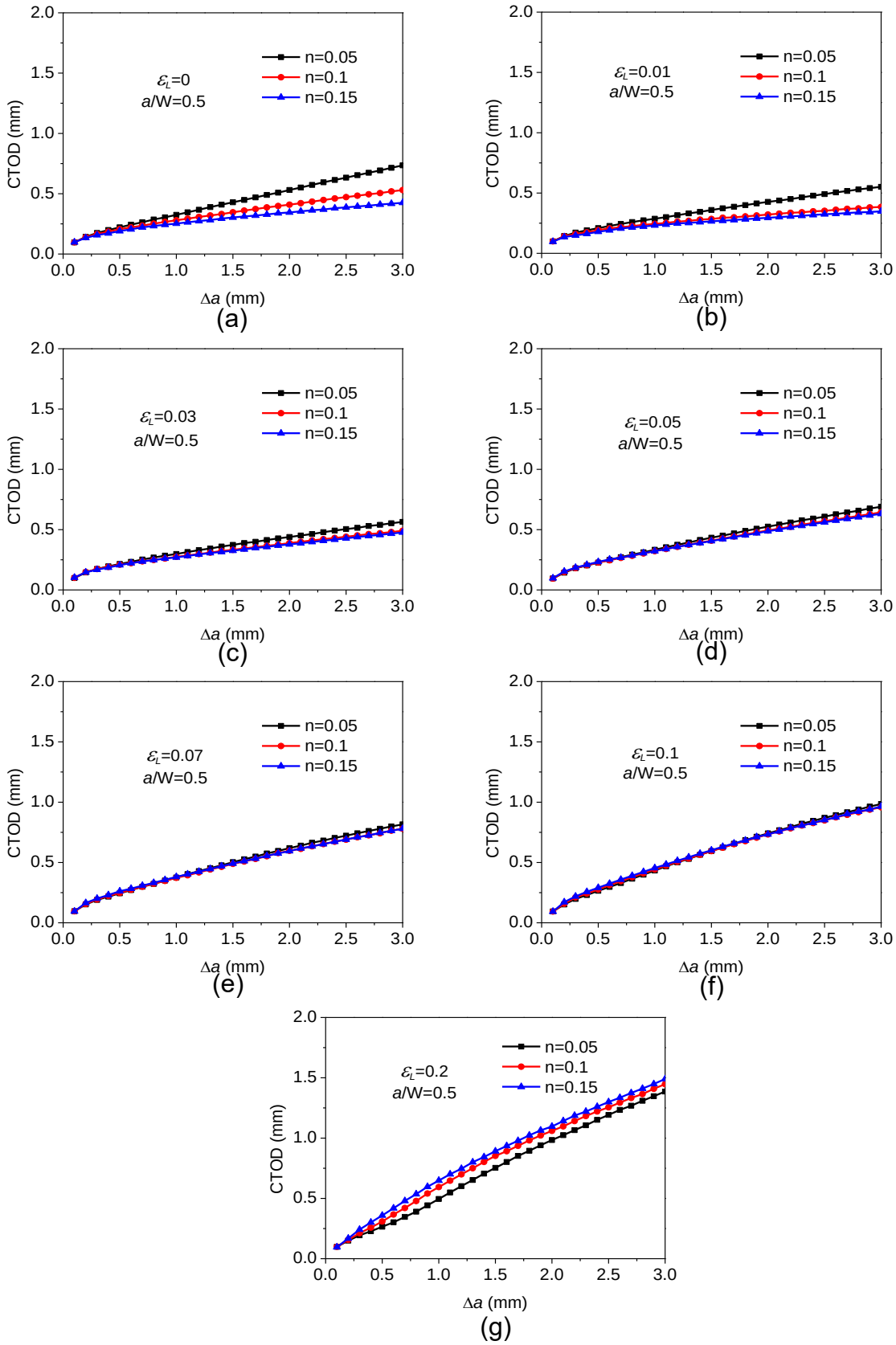

Fig. 15 Resistance curves for SENT specimens with $a/W = 0.5$ *and hardening exponent* $n = 0.05,\ 0.1,\ 0.15$. *(a)* $\varepsilon_L = 0$; *(b)* $\varepsilon_L = 0.01$; *(c)* $\varepsilon_L = 0.03$; *(d)* $\varepsilon_L = 0.05$; *(e)* $\varepsilon_L = 0.07$; *(f)* $\varepsilon_L = 0.1$; *(g)* $\varepsilon_L = 0.2$.

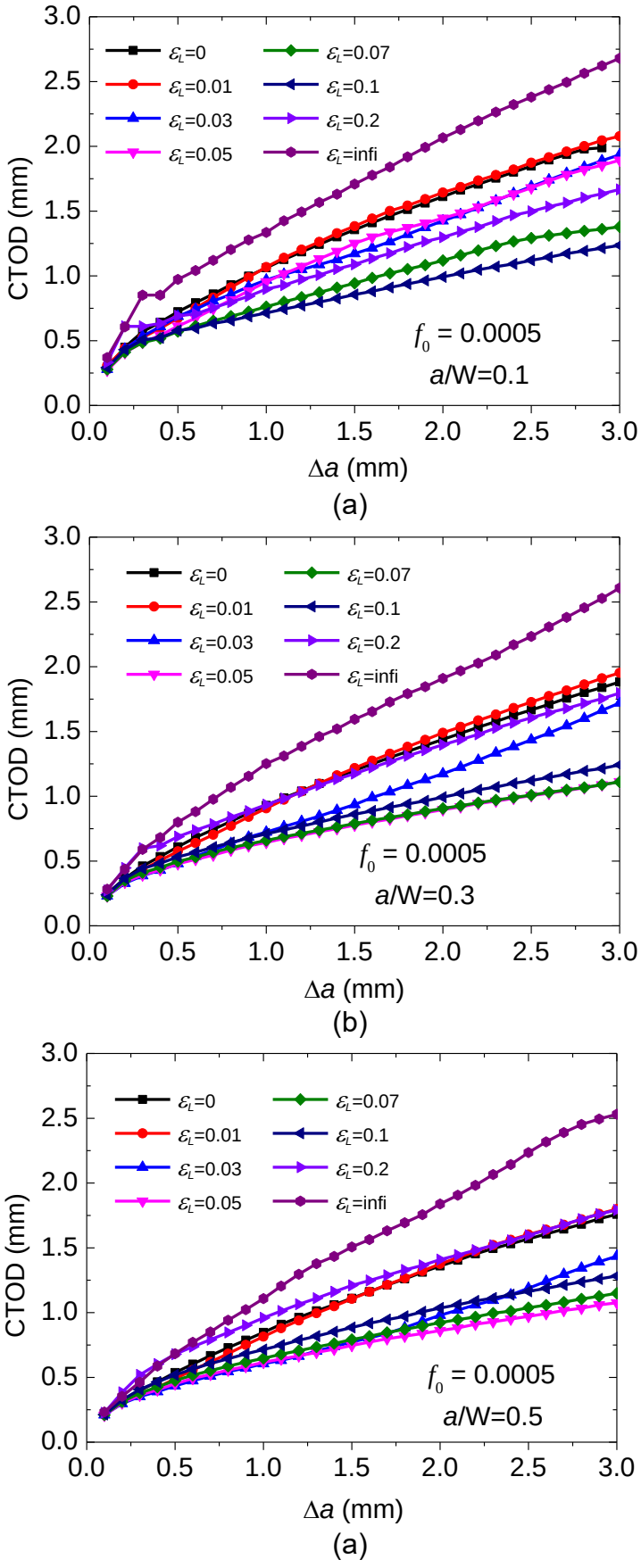

Fig. 16 The Lüders plateau length effect on the resistance curves of SENT specimens with $f_0 = 0.0005$ *and* $n = 0.05$*; (a) a/W=0.1; (b) a/W=0.3; (c) a/W=0.5.*

except $\varepsilon_L = \text{infi}$. Likewise, similar observations can be found in Fig. 16 (b) and (c), except $\varepsilon_L = 0.2$ for $a/W = 0.5$. In addition, values of ε_L corresponding to the lowest resistance curves for the same specimen geometry in Fig. 16 are larger than those in Fig. 4. Compared with the resistance curves in Fig. 4, it can be concluded that the Lüders plateau effect on resistance curves of materials with smaller initial void volume fraction are more pronounced. The existence of Lüders plateau reduces material's ductile crack resistance ability, which is not expected in engineering application for the integrity assessment.

5. Concluding remarks

In this study, we have investigated the Lüders plateau effect on ductile crack growth with two-dimensional SENT specimens in plane strain condition. The Gurson damage model is used to simulate the crack growth. A family of Lüders plateau length has been studied. It has been observed that the existence of Lüders plateau does not influence the initiation toughness but alters material's ductile fracture resistance. The Lüders plateau effect on ductile crack resistance curve depends on the crack depth. It has also been found that the Lüders plateau effect is controlled by the stress triaxiality ahead of the crack tip. The Lüders plateau effect is also observed for material with smaller initial void volume fraction and the effect is more pronounced. For materials with Lüders plateau, both the effects of crack depth and strain hardening on crack resistance curve are reduced. The larger the Lüders plateau is, the larger reduction will be.

Investigation on the Lüders plateau effect on crack driving force by Dahl have demonstrated that the existence of Lüders plateau intensified the crack driving force. Larger Lüders plateau corresponds to higher crack driving force (Dahl et al., 2018). Ductile crack growth lies in the competition of crack driving force and crack resistance. When the crack driving force is larger than material's crack resistance, ductile fracture proceeds; otherwise, fracture will be suppressed. Combining the results in (Dahl et al., 2018) and in this study, the Lüders plateau on one side increases the crack driving force; on the other side it may reduce material's ductile crack resistance, depending on the plateau length, crack depth, material's toughness and strain hardening. Attention should be paid for the application of materials with Lüders plateau, especially in the Arctic region.

Reference

Bai, Y., Teng, X., Wierzbicki, T., 2009. On the Application of Stress triaxiality formula for plane strain fracture testing. Journal of Engineering Material and Technology 131.

Bao, Y., Wierzbicki, T., 2004. On fracture locus in the equivalent strain and stress triaxiality space. International Journal of Mechanical Sciences 46, 81-98.

Beardsmore, D.W., da Fonseca, J.Q., Romero, J., English, C.A., Ortner, S.R., Sharples, J., Sherry, A.H., Wilkes, M.A., 2013. Study of Lüders phenomena in reactor pressure vessel steels. Materials Science and Engineering: A 588, 151-166.

Cravero, S., Ruggieri, C., 2005. Correlation of fracture behavior in high pressure pipelines with axial flaws using constraint designed test specimens—Part I: Plane-strain analyses. Engineering Fracture Mechanics 72, 1344-1360.

Dahl, B.A., Ren, X.B., Akselsen, O.M., Nyhus, B., Zhang, Z.L., 2018. Effect of low temperature tensile properties on crack driving force for Arctic applications. Theoretical and Applied Fracture Mechanics 93, 88-96.

Eikrem, P.A., Zhang, Z.L., Østby, E., Nyhus, B., 2008. Numerical study on the effect of prestrain history on ductile fracture resistance by using the complete Gurson model. Engineering Fracture Mechanics 75, 4568-4582.

Ermida, G., 2014. Strategic decisions of international oil companies: Arctic versus other regions. Energy Strategy Reviews 2, 265-272.

Gautier, D.L., Bird, K.J., Charpentier, R.R., Grantz, A., 2009. Assessment of undiscovered oil and gas in the Arctic. Science 324, 1175-1179.

Grange, M., Besson, J., Andrieu, E., 2000. An anisotropic gurson type model to represent the ductile rupture of hydrided zircaloy-4 sheets. International Journal of Fracture 105, 273-293.

Gurson, A.L., 1977. Continuum theory of ductile rupture by void nucleation and growth Part I—Yield criteria and flow rules for porous ductile media Journal of Engineering Material and Technology 99, 2-15.

Hallai, J.F., Kyriakides, S., 2011a. On the effect of Lüders bands on the bending of steel tubes. Part I: Experiments. International Journal of Solids and Structures 48, 3275-3284.

Hallai, J.F., Kyriakides, S., 2011b. On the effect of Lüders bands on the bending of steel tubes. Part II: Analysis. International Journal of Solids and Structures 48, 3285-3298.

Hallai, J.F., Kyriakides, S., 2013. Underlying material response for Lüders-like instabilities. International Journal of Plasticity 47, 1-12.

Han, J., Lu, C., Wu, B., Li, J., Li, H., Lu, Y., Gao, Q., 2017. Innovative analysis of Luders band behaviour in X80 pipeline steel. Materials Science and Engineering: A 683, 123-128.

Han, K.J., Shuai, J., Deng, X., Kong, L., Zhao, X., Sutton, M., 2014. The effect of constraint on CTOD fracture toughness of API X65 steel. Engineering Fracture Mechanics 124-125, 167-181.

Harsem, Ø., Eide, A., Heen, K., 2011. Factors influencing future oil and gas prospects in the Arctic. Energy Policy 39, 8037-8045.

Henry, B.S., Luxmoore, A.R., 1997. The stress triaxiality constraint and the Q-value as a ductile fracture parameter. Engineering Fracture Mechanics 57, 375-390.

Liu, Y., Kyriakides, S., Hallai, J.F., 2015. Reeling of pipe with Lüders bands. International Journal of Solids and Structures 72, 11-25.

Mazière, M., Luis, C., Marais, A., Forest, S., Gaspérini, M., 2017. Experimental and numerical analysis of the Lüders phenomenon in simple shear. International Journal of Solids and Structures 106-107, 305-314.

Nahshon, K., Hutchinson, J.W., 2008. Modification of the Gurson Model for shear failure. European Journal of Mechanics - A/Solids 27, 1-17.

Nourpanah, N., Taheri, F., 2011. Ductile crack growth and constraint in pipelines subject to combined loadings. Engineering Fracture Mechanics 78, 2010-2028.

O'Dowd, N.P., Shih, C.F., 1991. Family of crack-tip fields characterized by a triaxiality parameter—I. Structure of fields. Journal of the Mechanics and Physics of Solids 39, 981-1015.

O'Dowd, N.P., Shih, C.F., 1992. Family of crack-tip fields characterized by a triaxiality parameter—II. Fracture applications. Journal of the Mechanics and Physics of Solids 40, 939-963.

Østby, E., Thaulow, C., Zhang, Z.L., 2007a. Numerical simulations of specimen size and mismatch effects in ductile crack growth – Part I: Tearing resistance and crack growth paths. Engineering Fracture Mechanics 74, 1770-1792.

Østby, E., Thaulow, C., Zhang, Z.L., 2007b. Numerical simulations of specimen size and mismatch effects in ductile crack growth – Part II: Near-tip stress fields. Engineering Fracture Mechanics 74, 1793-1809.

Ren, X., Nordhagen, H.O., Zhang, Z., 2015. Tensile properties of 420MPa steel at low temperature, Twenty-fifth Internation Ocean and Polar Engineering Conference, Hawaii.

Tsuchida, N., Tomota, Y., Nagai, K., Fukaura, K., 2006. A simple relationship between Lüders elongation and work-hardening rate at lower yield stress. Scripta Materialia 54, 57-60.

Tu, S., Ren, X., He, J., Zhang, Z., 2018. Study of low temperature effect on the fracture locus of a 420 MPa structural steel with the edge tracing method. Fatigue & Fracture of Engineering Materials & Structures On line.

Tvergaard, V., 1981. Influence of voids on shear band instabilities under plane strain conditions. International Journal of Fracture 17, 389-407.

Tvergaard, V., 1982. On localization in ductile materials containing spherical voids. International Journal of Fracture 18, 237-252.

Tvergaard, V., Needleman, A., 1984. Analysis of the cup-cone fracture in a round tensile bar. Acta metall 32, 157-169.

Xia, L., Shih, C.F., 1995. Ductile crack growth-I. A numerical study using computational cells with microstructurally-based length scales. Journal of the Mechanics and Physics of Solids 43, 233-259.

Xia, L., Shih, C.F., Hutchinson, J.W., 1995. A computational approach to ductile crack growth under large scale yielding conditions. Journal of the Mechanics and Physics of Solids 43, 389-413.

Xu, J., Zhang, Z.L., Østby, E., Nyhus, B., Sun, D.B., 2009. Effects of crack depth and specimen size on ductile crack growth of SENT and SENB specimens for fracture mechanics evaluation of pipeline steels. International Journal of Pressure Vessels and Piping 86, 787-797.

Xu, J., Zhang, Z.L., Østby, E., Nyhus, B., Sun, D.B., 2010. Constraint effect on the ductile crack growth resistance of circumferentially cracked pipes. Engineering Fracture Mechanics 77, 671-684.

Zhang, Z., Thaulow, C., Ødegård, J., 2000. A complete Gurson model approach for ductile fracture. Engineering Fracture Mechanics 67, 155-168.

Zhang, Z.L., 1996. A sensitivity analysis of material parameters for for the Gurson constitutive model. Fatigue & Fracture of Engineering Materials & Structures 19, 561-570.

Zhang, Z.L., C., T., M., H., 1997. Effects of crack size and weld metal mismatch on the has cleavage toughness of wide plates. Engineering Fracture Mechanics 57, 653-664.

Zhang, Z.L., Hauge, M., Thaulow, C., 1996. Two parameter characterization of the near-tip stress field for a bi-material elastic-plastic interface crack. International Journal of Fracture 79, 65-83.

Zhao, L., Jing, H., Xiu, J., Han, Y., Xu, L., 2014. Experimental investigation of specimen size effect on creep crack growth behavior in P92 steel welded joint. Materials & Design 57, 736-743.